Multimodal Transportation 3 (2024) 100138

Contents lists available at ScienceDirect

Multimodal Transportation

journal homepage: www.elsevier.com/locate/multra

Ship refueling optimization for dual-fuel ships considering carbon intensity indicator rating limit and uncertain fuel prices

Yiwei Wu [a], Haoran Guo [b], Jingwen Qi [a,*], Shuaian Wang [a], Lu Zhen [c]

[a] Department of Logistics and Maritime Studies, The Hong Kong Polytechnic University, Hung Hom, Kowloon, Hong Kong 999077, China
[b] Department of Industrial Engineering, Tsinghua University, Beijing 100084, China
[c] School of Management, Shanghai University, Shanghai 200436, China

ARTICLE INFO

Keywords:
Ship refueling
Dual-fuel ships
Multistage stochastic programming
Scenario reduction
Carbon emission cost
CII rating

ABSTRACT

Refueling decisions of liner ships are facing challenges from both fuel price fluctuations and carbon emission constraints. This paper proposes a multistage stochastic programming model to tackle the refueling problem for dual-fuel ships under carbon intensity indicator (CII) rating limit and carbon tax costs. The model also takes into account various factors, including fuel consumption of main and auxiliary engines, fuel availability at ports of call, and fuel price fluctuations. The proposed model is solved using scenario size selection and moment matching methods, and a greedy heuristic algorithm is adopted to speed up the process. Managerial insights are obtained from multinomial logistic regression and sensitivity analyses. Our numerical results reveal that low sulfur fuel oil (LSFO) refueling decisions are closely linked to the difference of LSFO and liquefied natural gas (LNG) fuel prices and that LSFO becomes more attractive when the variance of LSFO fuel price or the LNG availability decreases. Besides, carbon emission costs are found to become a true consideration when carbon taxes exceed a certain threshold. These insights can help practitioners better understand the coupling influence of carbon emissions and fuel price fluctuations on the ship refueling problem.

1. Introduction

Liner shipping is an efficient and standardized mode of container cargo transportation. Its core characteristic is to adhere to fixed schedules and predetermined routes to ensure the cargo is transported as planned. Liner shipping companies proactively promote their service routes, including a schedule listing the sequence of ports of call, to attract customers to book their services (Meng et al., 2014). This mode of transportation relies on a strict timetable, ensuring that the ship arrives at the designated ports at the scheduled times. One of the major conveniences for customers is that the arrival dates of liner shipments are usually announced in advance and remain stable within a period of three to six months (Wang and Meng, 2012). This stability and predictability make liner shipping an important and reliable logistic choice in international trade.

Given the limited capacity of fuel tanks, even with a full tank, ships usually cannot complete their entire voyage, making refueling at specific ports necessary. For liner shipping companies, determining the specific locations and quantities for refueling during the voyage is crucial, as fuel costs account for a large portion of their total operating costs. According to Ronen (2011), if fuel prices reach $500/metric ton (MT), fuel costs can account for three-quarters of a liner ship's operational costs. In this case, if the fuel prices at each port remained constant, the decision-making process for refueling would be relatively simple. However, the reality is that fuel prices

* Corresponding author.
E-mail addresses: yiwei.wu@connect.polyu.hk (Y. Wu), ghr20@mails.tsinghua.edu.cn (H. Guo), jingwen.qi@connect.polyu.hk (J. Qi), hans.wang@polyu.edu.hk (S. Wang), lzhen@shu.edu.cn (L. Zhen).

https://doi.org/10.1016/j.multra.2024.100138
Received 12 May 2023; Received in revised form 13 January 2024; Accepted 26 March 2024

at individual ports can fluctuate greatly in the short term. For example, the average price of the very low sulphur fuel oil in global 20 ports soared from $875/MT in March to $1,126/MT in July 2022 (Ship and Bunker, 2024). Furthermore, considering the typically long voyages of liner shipping, fluctuations in fuel prices during the journey can be particularly severe. Such fluctuations in global oil prices introduce a significant degree of uncertainty into the operational management of liner shipping companies (Zhen et al., 2017). Therefore, studying the ship refueling decision-making process, taking into account the uncertainty of fuel prices at each port, holds significant practical importance (Wang et al., 2013).

In recent years, as global attention to the environmental impact of the maritime industry has continued to grow, the International Maritime Organization (IMO) has taken action to reduce greenhouse gas emissions from ships (IMO, 2018). Carbon emission policies, such as carbon tax, carbon quota, and carbon trading, have been proven to be effective means of reducing carbon emissions while promoting the sustainable development of the maritime industry (Jin et al., 2014). These policies have brought new challenges to the shipping operations management (Wang and Xu, 2015). Additionally, the maritime industry is seeking cleaner alternative marine fuels. Liquefied natural gas (LNG), as a popular clean fuel, has been proven to significantly reduce greenhouse gas emissions from ships (Wu et al., 2022). By 2018, 69% of LNG-fuel ships had installed dual-fuel engines (Zincir and Deniz, 2018). Therefore, choosing which type of fuel to bunker in ports becomes another critical decision for these dual-fuel ships. In summary, this paper considers dual-fuel ships that can use both low sulfur fuel oil (LSFO) and LNG, exploring the impact of this choice on the shipping operations management.

The remaining sections of this paper are organized as follows: Section 2 reviews the literature related to refueling decisions. Section 3 formulates a multistage stochastic programming model. Section 4 reports numerical experiment results and conducts sensitivity analyses. Section 5 includes contributions and future works of this paper.

2. Literature review

During the journey of liner ships, they may need to refuel at certain ports in order to continue their voyage (Wu et al., 2022). The refueling decision of a liner ship entails deciding where and how much to refuel in a given route. The refueling decision holds a crucial significance for liner shipping companies because the fuel cost constitutes a major portion of the total operational cost of a liner ship (Zhen et al., 2017). In general, the refueling decision depends on two main factors: fuel consumption and fuel prices (Zhen et al., 2017), both of which are considered in this paper. This section delves into the relevant literature pertaining to each of the two factors.

Firstly, numerous studies have extensively explored the various factors that impact ship fuel consumption, such as sailing speed, displacement, fuel type, and weather conditions. Fuel consumption is very sensitive to the sailing speed (Wang and Meng, 2012). Their relationship is often described by the cubic law, which states that a ship's bunker consumption in one unit of time is proportional to the cube of the sailing speed (Ronen, 1982). This law is commonly used in maritime studies, and several studies explore the precise exponent value in different contexts (e.g. Kontovas and Psaraftis (2011); Wang and Meng (2012)). For example, based on aggregated data from 2,259 container ships, Notteboom and Cariou (2009) find that the exponent value was approximately 3.3. Besides, how the ship's displacement affects the fuel consumption is examined (e.g. Bialystocki and Konovessis (2016)), and the influence of weather conditions on fuel consumption is also explored by several studies (e.g. Kosmas, Vlachos, 2008; Lin et al. (2013)). However, ship logging data containing weather condition data during the voyage is intrinsically fuzzy and inaccurate, and only conveys limited information (Meng et al., 2016), so we avoid including weather condition factors in our proposed model for brevity. Additionally, fuel consumption is closely related to the fuel type as well. There is a growing demand for cleaner alternative marine fuels (Wang et al., 2022; Ytreberg et al., 2021), with LNG emerging as a particularly popular choice. Notably, LNG can significantly reduce ship greenhouse gas emissions and is regarded as a clean fossil marine fuel (Wu et al., 2022). Against this backdrop, this paper investigates the refueling problem for dual-fuel liner ships, which can consume either traditional LSFO or environmentally friendly LNG.

Secondly, fuel prices fluctuate frequently over time in reality (Zhen et al., 2017)), complicating refueling decisions. Existing studies also consider the impact of fuel price fluctuations on the refueling decision. For example, Ghosh et al. (2015) examine a refueling decision problem that incorporates special contract issues regarding fuel prices, while Meng et al. (2015) investigate the routing decision problem in light of varying bunker prices at different ports. Given the similarities between the refueling decision problem and inventory replenishment problem, Sheng et al. (2015) propose an effective dynamic (s, S) policy and a sample average approximation method to solve the liner shipping problem under bunker prices and consumption uncertainties. Additionally, Zhen et al. (2017) use dynamic programming to address the refueling decision problem, incorporating stochastic parameters for fuel prices. Recently, Lashgari et al. (2021) develop a scenario-based stochastic linear integer programming model to jointly optimize routing, sailing speed, and bunkering policy under fuel price uncertainty.

Compared to the existing literature, the main contribution of this study is that this paper incorporates the carbon intensity indicator rating limit and uncertain fuel prices into the ship refueling optimization problem for dual-fuel ships, which to the best of our knowledge has not been explored in previous research. Specifically, this paper examines how fuel price fluctuations impact refueling amount decisions and fuel type choices for ships with dual-fuel engines. Moreover, the study explores how decision boundaries may vary due to fuel availability at ports of call and carbon taxes, providing managerial insights into the potential impact of carbon tax policies.

3. Problem description and model formulation

This study focuses on a ship refueling problem for dual-fuel ships, with the consideration of fuel consumption of both main and auxiliary engines, ship carbon emissions, availability of LNG at different ports of call, and uncertainty in fuel prices. This section first elaborates on the detailed background of the problem in Section 3.1, explains the objective function of the problem in Section 3.2, introduces multistage stochastic programming in Section 3.3, and formulates the mathematical model in Section 3.4.

3.1. Problem background

Assuming a liner company considers whether to charter a dual-fuel container ship and deploy the ship on a given ship route, the ship needs to visit a set I of ports of call on a fixed schedule with the aim of minimizing the total expected cost while maintaining a desired carbon intensity indicator (CII) rating. Over a planning horizon, the container ship needs to complete a set N of round trips for container transport. A service plan of the ship including sailing speed and arrival time has been already determined by the liner company. The dual-fuel container ship could consume either LSFO or LNG as marine fuel. Moreover, the ship contains a main engine providing propulsion power for the ship and an auxiliary engine providing power for uses except propulsion. This study assumes that the main engine can burn LSFO or LNG, and the auxiliary engine burns only LSFO. In addition, several ports of call in I can provide LSFO bunkering service, but only a few ports of call can provide LNG bunkering service because in real life, not all ports are equipped with LNG bunkering facilities. Hence, let I^F ($I^F \subset I$), and I^L ($I^L \subset I$) represent sets of all ports of call on the ship route where LSFO, and LNG are available, respectively. The ship can only refuel LSFO (or LNG) at ports of call where LSFO (or LNG) bunkering facilities are available.

Over a long planning horizon, fuel prices of LSFO and LNG always fluctuate across months. For example, crude oil price in global markets soared from around \$76/barrel in early January 2022 to over \$110/barrel by March 4, 2022 (GEP, 2022) following the Ukraine-Russia War. Hence, considering liner operations management under uncertainty in fuel prices brings our problem closer to reality. This means that optimal ship refueling decisions considering the uncertainty in fuel prices of both LSFO and LNG are of particular interest to the liner shipping industry because for liner companies, fuel costs account for more than half of the total operating cost (Fagerholt and Psaraftis, 2015). As the usual practice of the stochastic programming model formulation, the uncertainty in this study is represented by scenarios. Specifically, let S, and M represent the set of all scenarios indexed by s, and the set of all months in the planning horizon indexed by m, respectively. Besides, the uncertainty in the unit prices of LSFO and LNG is represented by a finite set of scenarios, which means that c^F_{ims}, and c^L_{ims} are defined as the unit prices of LSFO, and LNG at port of call i in month m under scenario s, respectively. The first important decision related to ship refueling is the inventory levels of LSFO and LNG when the ship arrives at each port. Let π^F_{nis}, and π^L_{nis} represent the ship LSFO inventory level, and the LNG inventory level when the ship arrives at port of call i of round trip n under scenario s. In this case, the value of $\pi^F_{n,i+1,s}$ ($\pi^L_{n,i+1,s}$) can be calculated by the value of π^F_{nis} (π^L_{nis}) plus the amount of LSFO (LNG) refueled at port of call i minus the fuel consumption of the ship sailing during the voyage from port of call i to port of call $i+1$ (also called leg i) and mooring at ith port of call.

At each port of call, the refueled amount of LSFO and LNG should be determined, which is the second ship refueling related decision. Bunkering time is ignored in this study because the container ship can be refueled while loading and unloading containers. For brevity, we assume that the fuel tank is refueled as soon as the ship arrives, if the ship is planned to refuel at this port of call. Let ε^F_{nis} and ε^L_{nis} represent the amount of LSFO and LNG refueled at port of call i of round trip n under scenario s, respectively. Obviously, the amount of fuel in tank after refueling should not exceed the tank capacity. The storage tanks for LSFO and LNG have a capacity of o^F and o^L, respectively.

The last decision related to ship refueling is the choice of fuel type used for each leg of each round trip, that is, whether the main engine uses LSFO or LNG. To this end, we define α_{nis} as a binary variable that equals 1 if the main engine of the ship consumes LSFO during leg i on the ship route of round trip n under scenario s, and 0 otherwise. The value of α_{nis} has a direct influence on the fuel consumption of the main engine for each leg. Specifically, most of the current fuel consumption models in the literature, such as Wang and Meng (2012), calculate the unit fuel consumption function by $k_1 v^{k_2}$, where v is the sailing speed (knot), and k_1 and k_2 are positive coefficients. However, in addition to sailing speed, displacement (i.e., the total weight of the ship itself, cargo, ballast water and bunker) also significantly influences fuel consumption (Meng et al., 2016). Hence, this study formulates the unit fuel consumption function of LSFO (LNG) as $k^F_1 v^{k^F_2} (d_{ni})^{k^F_3}$ ($k^L_1 v^{k^L_2} (d_{ni})^{k^L_3}$) (ton/hour), where k^F_1, k^F_2, and k^F_3 (k^L_1, k^L_2, and k^L_3) are positive coefficients for LSFO (LNG) consumption, and v and d_{ni} represent actual sailing speed (knot) and actual displacement of the ship during voyage i of round trip n (ton), respectively. Finally, in terms of fuel consumption of the auxiliary engine, we assume that the auxiliary engine of the ship consumes e amount of LSFO per hour, and that the total time of completing leg i, including sailing time of leg i and dwell duration at port of call i (hour), is t_i, indicating the total LSFO consumption of the auxiliary engine for $|N|$ round trips is $\sum_{n\in N}\sum_{i\in I} et_i$.

From 1 January 2023, all ships are required to report their annual operational CII and CII rating (IMO, 2022). In this case, liner companies need to consider the carbon emissions per unit transport work of each operating container ship, which is also known as the carbon intensity. One of the carbon intensity indicators is the Annual Efficiency Rating (AER) (g CO_2/dwt/nm) approved by the International Maritime Organization (IMO) as mandatory to calculate the total annual CO_2 emissions per deadweight mile sailed throughout the year to measure the energy efficiency level of each operating ship. Equation (1) is the calculation formula of AER, which is given by IMO (2011). In this study, let a represent the upper bound of the attained annual operational AER value for a desired rating. Then, the AER value of the container ship after completing $|N|$ round trips in a one-year planning horizon needs to

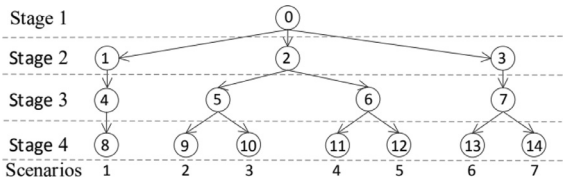

Fig. 1. Illustration of a scenario tree.

satisfy the upper bound.

$$\text{AER} = \frac{\text{total carbon emissions of the ship during ballast and laden voyages (g)}}{\text{deadweight tonnage} \times \text{total distance}}. \tag{1}$$

3.2. Objective function

The objective of this problem is to minimize the total expected cost in the planning horizon, which contains only carbon emission and fuel purchase costs because other costs are constant in this study. The first cost in the objective function is the annual carbon emission cost. As introduced in Section 3.1, the carbon emission cost contains carbon emission costs from LSFO and LNG. We first show how to calculate the annual carbon emission cost from LNG consumption because this item is simpler than that from LSFO. As this study formulates the unit fuel consumption function for LNG consumption as $k_1^L v^{k_2^L} (d_{ni})^{k_3^L}$ (ton/hour), the annual LNG consumption is $(1-\alpha_{nis})(k_1^L v^{k_2^L} (d_{ni})^{k_3^L} \frac{l_i}{v})$, where l_i represents the length (n mile) of the ith leg on the ship route, implying the expected annual carbon emission cost from LNG is $\sum_{n\in N}\sum_{i\in I}\sum_{s\in S} w_s p g_L (1-\alpha_{nis})(k_1^L v^{k_2^L} (d_{ni})^{k_3^L} \frac{l_i}{v})$, where w_s, p, and g_L represent the probability of scenario s, carbon tax per ton (USD/ton), and the amount of CO_2 generated when burning one ton of LNG (ton), respectively. Similarly, the annual LSFO consumption for the main engine is $\sum_{n\in N}\sum_{i\in I}\sum_{s\in S}(\alpha_{nis} k_1^F v^{k_2^F} (d_{ni})^{k_3^F} \frac{l_i}{v})$. And the annual LSFO consumption for the auxiliary engine is $\sum_{n\in N}\sum_{i\in I} et_i$. Hence, the expected annual carbon emission cost from LSFO is $\sum_{n\in N}\sum_{i\in I}\sum_{s\in S} w_s p g_F (\alpha_{nis} k_1^F v^{k_2^F} (d_{ni})^{k_3^F} \frac{l_i}{v} + et_i)$, where g_F represent the amount of CO_2 generated when burning one ton of LSFO (ton).

The second cost in the objective function is the annual expected fuel purchase cost, which can be calculated by $\sum_{n\in N}\sum_{i\in I}\sum_{s\in S} w_s j_{nim} (c_{ims}^F \varepsilon_{nis}^F + c_{ims}^L \varepsilon_{nis}^L)$, where j_{nim} is an auxiliary parameter, and it equals 1 if and only if port of call i of round trip n is visited in month m and equals 0 otherwise. Hence, the objective function of this problem is formulated as

$$\sum_{n\in N}\sum_{i\in I}\sum_{s\in S} w_s \left(p(g_F(\alpha_{nis} k_1^F v^{k_2^F} d_{ni}^{k_3^F} \frac{l_i}{v} + et_i) + g_L(1-\alpha_{nis})(k_1^L v^{k_2^L} d_{ni}^{k_3^L} \frac{l_i}{v})) + j_{nim}(c_{ims}^F \varepsilon_{nis}^F + c_{ims}^L \varepsilon_{nis}^L) \right).$$

3.3. Multistage stochastic programming

Given the consideration of uncertain fuel prices in this study, it is necessary to employ an appropriate mathematical method to handle these uncertain parameters. In current literature, two-stage stochastic programming based on discrete probability distributions is widely used to address the uncertain fuel price issue. But for the specific uncertain environment we face, multistage stochastic programming may be more suitable. This is because, in two-stage stochastic programming, all information about uncertainty is assumed to be realized after the decision-making in the first stage, which does not align with our case. In our setting, shipping company managers typically only know the exact fuel prices for a certain period and the probability distribution of fuel prices for the period immediately following their decision-making moment, rather than the exact prices for all future periods. Therefore, this study employs multistage stochastic programming, where the uncertainty of each given stage is only revealed after the decision-making of the previous stage. For more information on multistage stochastic programming, please refer to Birge and Louveaux (2011).

In multistage problems, a scenario tree is commonly used to generate scenarios, which represents the branching process that occurs as stochastic progress is gradually observed. Fig. 1 presents a sample scenario tree with four periods and seven scenarios, with an artificial root node in stage 1. As each new stage is reached, additional realizations of uncertain fuel prices are represented by new nodes, leading to a unique path from the root to a leaf node in the last period, resulting in a total of seven scenarios. Therefore, a scenario in a multistage stochastic programming model corresponds to a path from the root node to a leaf node.

For multistage problems, nonanticipativity constraints must be added to ensure that the decisions in a certain period depend only on the data revealed up to that period but not on the information which will be realized in the future (Adulyasak et al., 2015). In other words, in this study, decision variables, including fuel inventory level, fuel usage option of the main engine, and the amount of fuel refueled, in a period of two different scenarios should be identical if the two scenarios share the same parent node in the scenario tree during the period.

3.4. Model formulation

Based on the above analyses, we can formulate a linear MIP stochastic programming model in this section. Note that this study further assumes that the ship's dwell time at each port of call on the route is deterministic. The notations mentioned in this model are listed as follows.

Sets and indices	
I:	set of all ports of call (legs) on the ship route, $i \in I$.
I^F:	set of all ports of call (legs) on the ship route where LSFO is available, $I^F \subset I$.
I^L:	set of all ports of call (legs) on the ship route where LNG is available, $I^L \subset I$.
M:	set of all months in the planning horizon, $m \in M$.
N:	set of all round trips completed by the ship in the planning horizon, $n \in N$.
S:	set of all scenarios, $s \in S$.
Z_+:	set of all non-negative integers.
Parameters	
a:	upper bound of the attained annual operational AER value for a desired rating.
c^F_{ims}:	unit price of LSFO at port of call i ($i \in I^F$) in month m ($m \in M$) under scenario s ($s \in S$) (USD/ton).
c^L_{ims}:	unit price of LNG at port of call i ($i \in I^L$) in month m ($m \in M$) under scenario s ($s \in S$) (USD/ton).
d_{ni}:	actual displacement of the ship during voyage i of round trip n (ton).
e:	amount of LSFO consumed by the auxiliary engine of the ship per hour (ton/hour).
f_{ns}:	index of node in the scenario tree in round trip n related to scenario s.
g_F:	amount of CO_2 generated when burning one ton of LSFO (ton).
g_L:	amount of CO_2 generated when burning one ton of LNG (ton).
h:	deadweight tonnage of the ship.
j_{nim}:	auxiliary parameter, if and only if port of call i of round trip n is visited in month m, it equals 1, otherwise it equals 0.
k^F_1, k^F_2, k^F_3:	positive coefficients for LSFO consumption (ton/hour).
k^L_1, k^L_2, k^L_3:	positive coefficients for LNG consumption (ton/hour).
l_i:	length (n mile) of the ith ($i \in I$) leg on the ship route.
o^F:	capacity of the tank for storing LSFO.
o^L:	capacity of the tank for storing LNG.
p:	carbon tax per ton (USD/ton).
t_i:	total time of completing leg i, including sailing time of leg i and dwell duration at port of call i on the ship route (hour).
v:	sailing speed of the deployed ship.
w_s:	probability of scenario s.
Variables	
α_{nis}:	binary, equals 1 if the main engine of the ship consumes LSFO during leg i under scenario s, on the ship route of round trip n; 0 if it consumes LNG.
ε^F_{nis}:	continuous, amount of LSFO refueled at port of call i of round trip n under scenario s (ton).
ε^L_{nis}:	continuous, amount of LNG refueled at port of call i of round trip n under scenario s (ton).
π^F_{nis}:	continuous, ship LSFO inventory level when the ship arrives at port of call i of round trip n under scenario s (ton).
π^L_{nis}:	continuous, ship LNG inventory level when the ship arrives at port of call i of round trip n under scenario s (ton).
$\tilde{\alpha}_{n,i,f_{ns}}$:	binary, variable α_{nis} related to the node f_{ns}.
$\tilde{\varepsilon}^F_{n,i,f_{ns}}$:	continuous, variable ε^F_{nis} related to the node f_{ns}.
$\tilde{\varepsilon}^L_{n,i,f_{ns}}$:	continuous, variable ε^L_{nis} related to the node f_{ns}.
$\tilde{\pi}^F_{n,i,f_{ns}}$:	continuous, variable π^F_{nis} related to the node f_{ns}.
$\tilde{\pi}^L_{n,i,f_{ns}}$:	continuous, variable π^L_{nis} related to the node f_{ns}.

Mathematical model

Based on the above definition of parameters and variables, a linear MIP model is formulated as follows.

$$\min \sum_{n\in N}\sum_{i\in I}\sum_{s\in S} w_s\left(p(g_F(\alpha_{nis}k^F_1 v^{k^F_2} d^{k^F_3}_{ni}\frac{l_i}{v}+et_i)+g_L(1-\alpha_{nis})(k^L_1 v^{k^L_2} d^{k^L_3}_{ni}\frac{l_i}{v}))+j_{nim}(c^F_{ims}\varepsilon^F_{nis}+c^L_{ims}\varepsilon^L_{nis})\right) \tag{2}$$

subject to:

$$\frac{\sum_{n\in N}\sum_{i\in I}10^6[g_F(\alpha_{nis}k^F_1 v^{k^F_2} d^{k^F_3}_{ni}\frac{l_i}{v}+et_i)+g_L(1-\alpha_{nis})k^L_1 v^{k^L_2} d^{k^L_3}_{ni}\frac{l_i}{v}]}{\sum_{n\in N}\sum_{i\in I} hl_i} \le a \qquad \forall s\in S \tag{3}$$

$$\varepsilon^F_{nis} \le o^F - \pi^F_{nis} \qquad \forall n\in N, i\in I^F, s\in S \tag{4}$$

$$\varepsilon^F_{nis} = 0 \qquad \forall n\in N, i\in I\backslash I^F, s\in S \tag{5}$$

$$\varepsilon^L_{nis} \le o^L - \pi^L_{nis} \qquad \forall n\in N, i\in I^L, s\in S \tag{6}$$

$$\varepsilon^L_{nis} = 0 \qquad \forall n\in N, i\in I\backslash I^L, s\in S \tag{7}$$

$$\pi^F_{1,1,s} = 0 \qquad \forall s \in S \tag{8}$$

$$\pi^L_{1,1,s} = 0 \qquad \forall s \in S \tag{9}$$

$$\pi^F_{n,i+1,s} = \pi^F_{nis} + \varepsilon^F_{nis} - \alpha_{nis} k^F_1 v^{k^F_2} d^{k^F_3}_{ni} \frac{l_i}{v} - et_i \qquad \forall n \in N, i \in \{1, \cdots, |I|-1\}, s \in S \tag{10}$$

$$\pi^L_{n,i+1,s} = \pi^L_{nis} + \varepsilon^L_{nis} - (1-\alpha_{nis}) k^L_1 v^{k^L_2} d^{k^L_3}_{ni} \frac{l_i}{v} \qquad \forall n \in N, i \in \{1, \cdots, |I|-1\}, s \in S \tag{11}$$

$$\pi^F_{n+1,1,s} = \pi^F_{n,|I|,s} + \varepsilon^F_{n,|I|,s} - \alpha_{n,|I|,s} k^F_1 v^{k^F_2} d^{k^F_3}_{n,|I|} \frac{l_{|I|}}{v} - et_{|I|} \qquad \forall n \in \{1, \cdots, |N|-1\}, s \in S \tag{12}$$

$$\pi^L_{n+1,1,s} = \pi^L_{n,|I|,s} + \varepsilon^L_{n,|I|,s} - \left(1-\alpha_{n,|I|,s}\right) k^L_1 v^{k^L_2} d^{k^L_3}_{n,|I|} \frac{l_{|I|}}{v} \qquad \forall n \in \{1, \cdots, |N|-1\}, s \in S \tag{13}$$

$$\alpha_{nis} = \tilde{\alpha}_{n,i,f_{ns}} \qquad \forall n \in N, i \in I, s \in S \tag{14}$$

$$\varepsilon^F_{nis} = \tilde{\varepsilon}^F_{n,i,f_{ns}} \qquad \forall n \in N, i \in I, s \in S \tag{15}$$

$$\varepsilon^L_{nis} = \tilde{\varepsilon}^L_{n,i,f_{ns}} \qquad \forall n \in N, i \in I, s \in S \tag{16}$$

$$\pi^F_{nis} = \tilde{\pi}^F_{n,i,f_{ns}} \qquad \forall n \in N, i \in I, s \in S \tag{17}$$

$$\pi^L_{nis} = \tilde{\pi}^L_{n,i,f_{ns}} \qquad \forall n \in N, i \in I, s \in S \tag{18}$$

$$\alpha_{nis},\ \tilde{\alpha}_{n,i,f_{ns}} \in \{0,1\} \qquad \forall n \in N, i \in I, s \in S \tag{19}$$

$$\varepsilon^F_{nis}, \varepsilon^L_{nis}, \pi^F_{nis}, \pi^L_{nis}, \tilde{\varepsilon}^F_{n,i,f_{ns}}, \tilde{\varepsilon}^L_{n,i,f_{ns}}, \tilde{\pi}^F_{n,i,f_{ns}}, \tilde{\pi}^L_{n,i,f_{ns}} \geq 0 \qquad \forall n \in N, i \in I, s \in S. \tag{20}$$

Objective (2) aims to minimize the total annual cost, which includes the annual cost of fuel purchases and the annual cost of carbon emissions. Constraints (3) ensure that the ship's carbon intensity receives a desirable rating after completing $|N|$ round trips. Constraints (4–5) restrict refueling to LSFO at ports of call with LSFO bunkering facilities and limit the amount of LSFO in the tank after refueling to the LSFO tank capacity. Constraints (6–7) restrict refueling to LNG at ports of call with LNG bunkering facilities and limit the amount of LNG in the tank after refueling to the LNG tank capacity. Constraints (8–9) establish that the initial LSFO inventory level and the initial LNG inventory level are zero when the ship arrives at the first port of call of the first round trip. Constraints (10–13) compute the remaining LSFO amount and the remaining LNG amount of the ship at the next port of call. Constraints (15–19) are the nonanticipativity constraints adopted in this study. Constraints (20–21) define the decision variable ranges.

4. Computational experiments

To assess the proposed model, we conduct numerous experiments on a PC with 6 CPU cores, 2.6 GHz processing speed, and 24.0 GB memory. We implement the mathematical model using the off-the-shelf solver Gurobi 9.5.0 (Anaconda, Python). The parameters are set as outlined in Section 4.1, and the experimental results are presented in Section 4.2, followed by sensitivity analyses for managerial insights in Section 4.3.

4.1. Experimental setting

Assuming we consider the operation management of a container ships with a deadweight tonnage of 218,000 in 2023, according to ClassNK (2021), the value of a is set to $0.83 \times 0.95 \times 1984 \times 218000^{-0.489} \approx 3.836$. Sailing distance data, i.e., l_i, are obtained from the standard instances LINER-LIB (Brouer et al., 2013). As the minimal and maximal prices of intermediate fuel oil 380 (IFO380) in global 20 ports in 2022 are \$434.0, and \$769.5/ton, respectively (Ship and Bunker), the value of LSFO's unit price (i.e., c^F_{ims}) is set to be uniformly distributed over \$[400, 800]/ton. Besides, the LNG bunkering price paid by liner companies is set to \$800/ton in Wang et al. (2022), so we set the average value of LNG's unit price (i.e., c^L_{ims}) to \$800/ton (normal distribution with standard

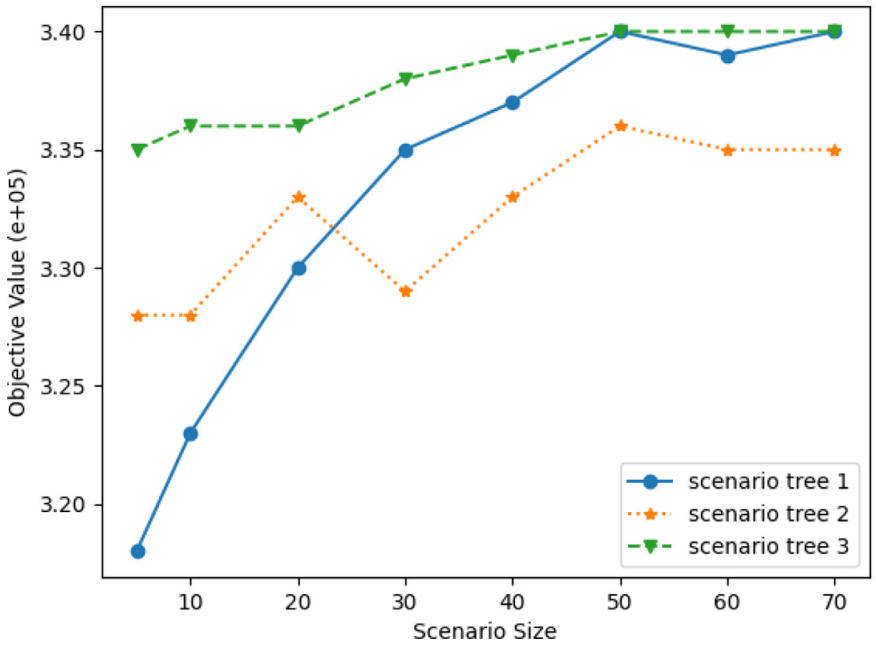

Fig. 2. Stability test of scenario size.

deviation \$100/ton). The value of sailing speed (i.e., v) is set to 15 knots, which is consistent with the setting in previous studies (Zhen et al., 2020). Regarding the set I^F (or I^L), we randomly select 3 (or 1) ports of call as ports which can provide LSFO (or LNG) bunkering services if the total number of ports of call is less than 5, and randomly select 7 (or 2) ports of call as ports which can provide LSFO (or LNG) bunkering services if the total number of ports of call is less than 10 but larger than 5 (the first port of call should provide bunkering service of at least one fuel type). Values of e, p, g_F, and g_L are set to 0.125 ton/hour, \$47.31/ton, 3.114 ton, and 2.750 ton, respectively, which is in line with the setting in Wu et al. (2022). Values of the LSFO tank capacity and the LNG tank capacity are set to 3,500 and 2,556 tons, respectively, which is in line with the setting in Zhen et al. (2017) and the tank capacity of a realistic container ship (Pekic, 2022). The dwell duration at each port of call is randomly selected from (24, 48) hours. The value of the actual displacement of the ship during each leg is set to be normally distributed with the mean of 200,000 tons and the standard deviation of 3,000, which is consistent with the setting in Wu et al. (2023). Values of k_1^F, k_2^F, and k_3^F are set to 0.00022, 2.5506, and 0.2072, respectively, which is in line with the setting in Meng et al. (2016). According to ABS (2020), LNG is about half the density of heavy fuel oil but has about 20 percent higher calorific value, and it takes about 1.8 times as much LNG to achieve the same distance compared to fuel oil on a volume (m^3) basis. Therefore, values of k_1^F, k_2^F, and k_3^F are set to 0.000198, 2.5506, and 0.2072, respectively.

4.2. Scenario generation and reduction

4.2.1. Scenario size selection

Normally, multistage stochastic models are solved with generated discrete scenarios representing possible realizations of uncertainty. However, things become complex when it comes to a stochastic model with continuous random parameters, since the continuous distributions have to be properly approximated by discrete distributions with a finite number of scenarios in order to be tractable (Feng and Ryan, 2013).

To decide the scenario size (how many discrete scenarios to generate for each continuous distribution at each stage, i.e. how many branches are there in each node of the scenario tree), stability analysis is required, featuring the trade-off between the representation quality of discrete scenarios and the computation burden. We take a route with four ports of call as an example, where the ship starts from Kaohsiung, arrives at General Santos City and Manila sequentially, and finally returns to Kaohsiung. Stochastic solutions are generated under each scenario tree with certain scenario size ranging from 5 to 70, and the objective values obtained by the model in Section 3.4 are recorded. To ensure the robustness of the stability analysis, for each scenario size, three scenario trees are generated independently under different random seeds, and the results are shown in Fig. 2. It turns out that as the scenario size grows, the objective value first increases and then becomes stable when the scenario size is larger than 50. This phenomenon is reasonable because when the scenario size is small, discrete scenarios are more likely to concentrate around the mean value of continuous distribution, thus missing some possible extreme values, making the derived objective values appear over-optimistic. With more different cases considered, discrete scenarios incorporate a more accurate representation of the continuous distribution, and

Table 1
Weak out-of-sample stability test of scenario size.

Solution	Objective value under Tree 1 (e+05)	Objective value under Tree 2 (e+05)	Objective value under Tree 3 (e+05)	Objective value under Tree 4 (e+05)
1	3.28	3.52	3.58	3.76
2	3.51	3.33	3.73	3.89
3	3.57	3.75	3.37	3.74
4	3.66	3.76	3.72	3.18

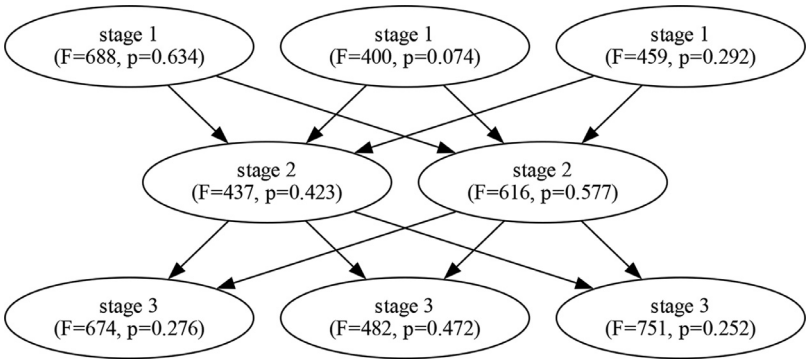

Fig. 3. An example of generated scenario tree.

objective values become stable and robust to the scenario size. As suggested by Fig. 2, an appropriate scenario size is 50 for this route with four ports of call. Note that as the port number changes, the corresponding recommended scenario size may also change.

Furthermore, the out-of-sample stability test is conducted because one cannot simply compare solutions from different trees, as different scenario settings may lead to various objective values (Heitsch and Römisch, 2003). Following the weak out-of-sample stability test procedure of Hu and Hu (2018), we generate four scenario trees with scenario size 50, obtain the stochastic solutions under these four trees, and test their performance (i.e. objective value) under the scenario setting of other trees, with the test result shown in Table 1.

For a scenario size that is large enough, we expect the performance of solution i under tree j to approximate the performance of solution j under tree i (Hu and Hu, 2018). In our result, the maximum gap is 3.34%, indicating a valid scenario size.

4.2.2. *Moment matching method*

Based on the chosen scenario size, we adopt the moment matching method proposed by Høyland and Wallace (2001) to determine probability mass for the generated discrete scenarios, aiming to make the moments of discrete scenarios match those of the original continuous distributions. The moment matching process incorporates a nested optimization problem before solving the main stochastic programming, as stated below:

$$\min_{p} \sum_{\phi \in \Phi} w_\phi (f_\phi(x,p) - VAL_\phi)^2 \tag{21}$$

subject to:

$$\sum_{i \in S} p_i = 1, \quad p_i \geq 0, \forall i \in S, \tag{22}$$

where S represents the set of discrete sample indexes, Φ represents the set of all statistical properties that we are interested in, w_ϕ is the weight we put in the statistical property ϕ, x_is are the random realizations of the continuous random vector X in the stochastic model, p_is are the decision variables in the nested optimization problem, f_ϕ represents the mathematical expression for statistical property ϕ, such as $f_{mean}(x,p) = \sum_{i \in S} p_i x_i$ for mean, and $f_{var}(x,p) = \sum_{i \in S} p_i (x_i - \sum_{j \in S} p_j x_j)^2$ for variance, and VAL_ϕ represents the target value of statistical property ϕ, i.e. the moments of the original continuous distribution.

As Hu and Hu (2018) suggested, since fuel prices are normal random variables in our model, we focus on the mean and variance when determining the optimal probability assignment. We still take the route with four ports of call as an example. Every time the ship arrives at a new port, scenarios about local fuel prices with size n_s are independently drawn from their continuous distributions, generating total scenarios with size $n_s^{|I| \times |N|}$, where n_s is denoted as scenario size in the following discussion, I is the set of all ports of call in the route, and N is the set of round trip indexes for the ship. Scenarios with a probability lower than 0.05 are eliminated from the tree and their probability masses are evenly re-distributed to those surviving scenarios, which serves as a heuristic way to conduct scenario reduction. Since we assume the fuel prices are time-independent and the observed prices at ports of call are uncorrelated with each other, we can construct the global scenario tree by fully connecting the fuel price realizations at different stages. Fig. 3 is an example of the generated scenario tree with $3 \times 2 \times 3 = 18$ possible scenarios after probability re-assignment, where F is the

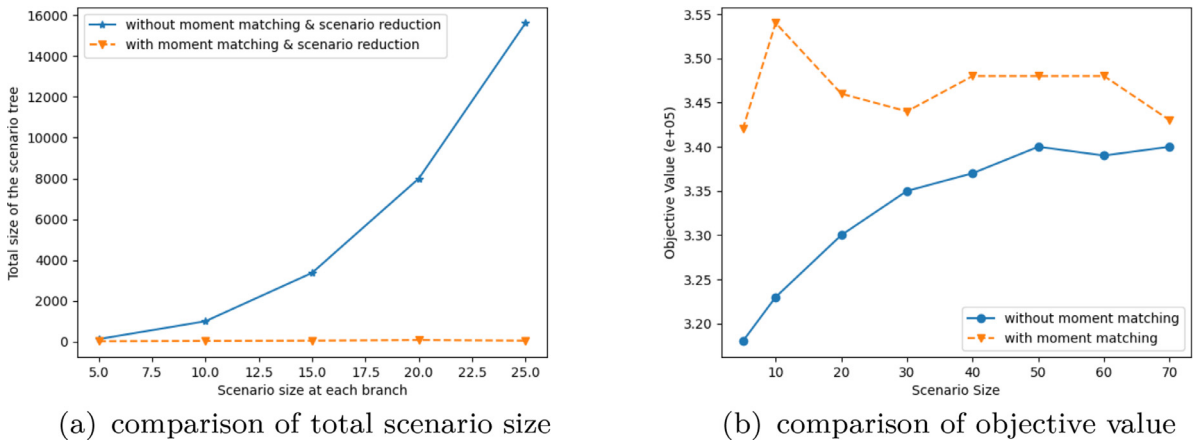

Fig. 4. Comparisons of total scenario size and objective value.

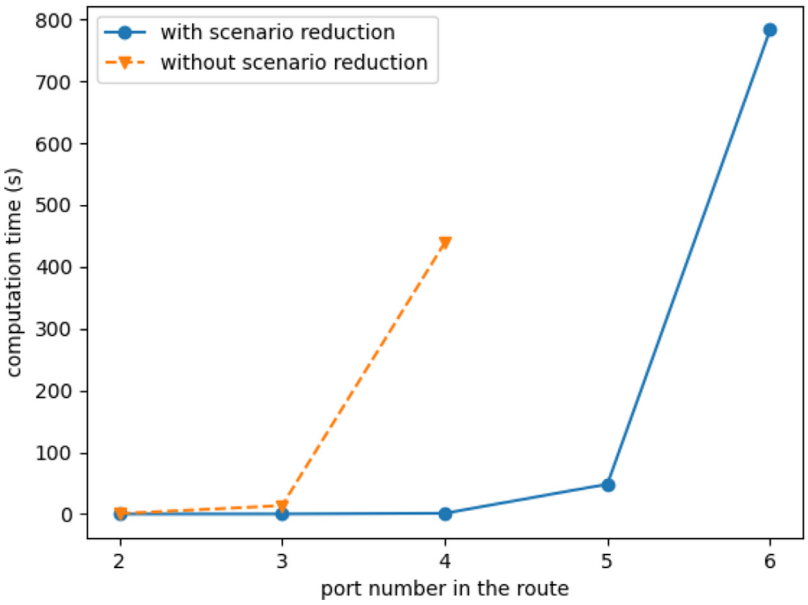

Fig. 5. How the computation time exponentially climbs despite the scenario reduction.

abbreviation of the price of fuel LSFO. Note that if two scenarios share the same node in stage s of the generated scenario tree, the corresponding fuel price of the two scenarios in stage s will be the same.

Moment matching and scenario reduction also introduce a trade-off between computation burden and solution quality. Since moments only carry partial information of the true distribution, the weighted discrete scenarios generated by moment matching and scenario reduction tend to be a worse representation of the true continuous distribution when compared with the results obtained by direct sample average algorithm (SAA) (Kleywegt et al., 2001). However, due to the exponential growth of the total scenario size in SAA, it is necessary to reduce the scenario size at the cost of losing some representation accuracy in order to make the method computationally tractable (Sha, et al., 2021). The comparisons of total scenario size and objective value before and after moment matching and scenario reduction for the route with four ports of call are shown in Fig. 4, where the solid curve represents before-reduction case, dashed curve represents after-reduction case, and the x-axis represents the scenario size (at each branch).

However, despite the capacity of moment matching and scenario reduction, it is still implausible to handle the scenario tree for routes with substantial ports of call, since a nonlinear and non-convex optimization problem has to be solved to determine the optimal probability mass distribution in the moment matching method when we consider moments with order higher than two. As the number of ports of call increases, the initial number of total scenarios before reduction will surge exponentially, making the moment matching and scenario reduction themselves too time-consuming. Fig. 5 shows how the moment matching fails for routes with large port number, with the scenario size fixed to be only 20. Note that as the port number grows larger than four, the model solving time without moment matching and scenario reduction surges longer than 30 minutes, which fails to be shown in the figure.

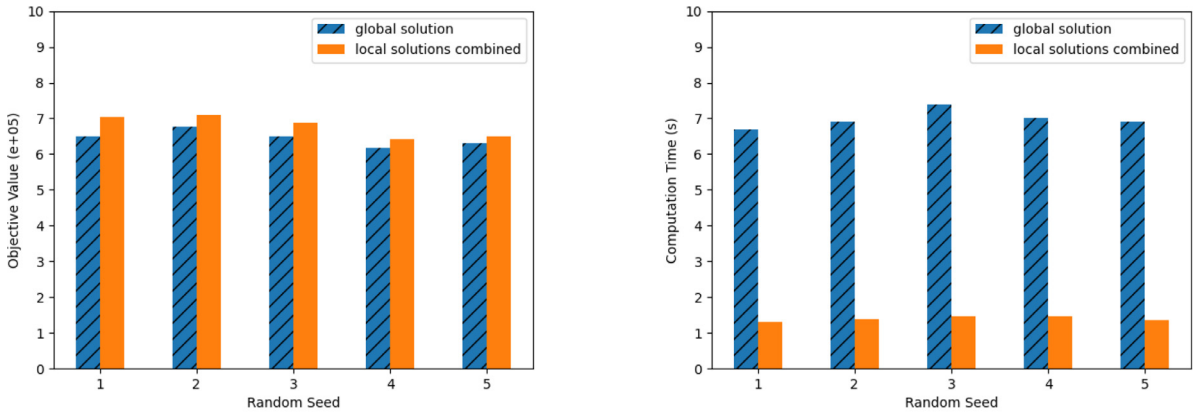

Fig. 6. Comparisons of global solution and greedy local solutions.

Table 2
Sample mean of LSFO fuel prices under different refueling decisions.

Refueling decision	Sample mean of LSFO fuel price
0	694.6
1	648.3
2	561.4
3	461.8

Hence, we propose a heuristic greedy method to obtain stochastic solutions for long routes, which is to decompose the global refueling decision into the aggregation of several local refueling decisions. The assumption we based on is the independence of fuel prices between different ports and different time as mentioned in the experiment setting, as it ensures that several sub-scenario trees can be generate independently after the decomposition. Then several local optimal stochastic solution sets can be obtained by the methods mentioned before, and a feasible global solution can be obtained by the direct aggregation. Since only part of the whole solution space is explored, with those extremely radical refueling decisions (refuel for the following many legs) not considered, the ultimate solutions are not guaranteed to be globally optimal. However, they are often satisfactory solutions. Fig. 6 is an example of the comparisons between proposed heuristic solutions and global optimal solutions where a 6-port route is considered and decomposed into 2 sub-routes. On average, greedy local solutions save 79.94% computation time while only increase 5.16% objective value compared with global optimal solutions, which is satisfactory for a quick heuristic method.

4.2.3. Analysis of the stochastic solution value

In this section, we examine whether considering the uncertainty is necessary by computing the Value of Stochastic Solution (VSS). To derive VSS, we should get deterministic and stochastic solutions respectively. Stochastic solutions are obtained by solving the aforementioned stochastic model. Deterministic solutions can be obtained by solving the deterministic model constructed by replacing the random parameters with their expected values in the stochastic model. Then both solutions are tested under the same scenario tree, and the difference between the performance of deterministic solutions and stochastic solutions is the required VSS.

Take the route with four ports of call as an example, we set the scenario size to be 50 with moment matching and scenario reduction conducted. The objective values of both solutions under different random seeds are shown in the Fig. 7. The relative VSS is 12.44% on average, with the absolute VSS being $46,800, quantifying the value of considering uncertainty in this case.

4.3. Sensitivity analysis and management insights

4.3.1. Soft decision boundary by multinomial logistic regression

For the following discussion, we take the route with four ports of call as a proper and convenient analytic unit, because it suffices to provide insights into long routes, while maintains a tractable computation burden. We take the LSFO refueling decision at port 1 in the route as an example to illustrate the influence of fuel prices on decisions, as only port 1 can be completely free from the confounding influence of previous decisions, thus focusing on the impact of local fuel prices on decisions.

Since the choices of LSFO and LNG are mutually exclusive and LSFO is often preferred than LNG in the majority of generated scenarios, we simply focus on the decision of LSFO refueling. As shown in Fig. 8 where different colors represent different fuel decisions, the lower the fuel price of LSFO at port 1, the more likely we are to refuel more LSFO for the ship at port 1. The sample means of LSFO fuel price at port 1 under different decisions and Welch's t-test results are shown in Table 2 and 3, supporting the

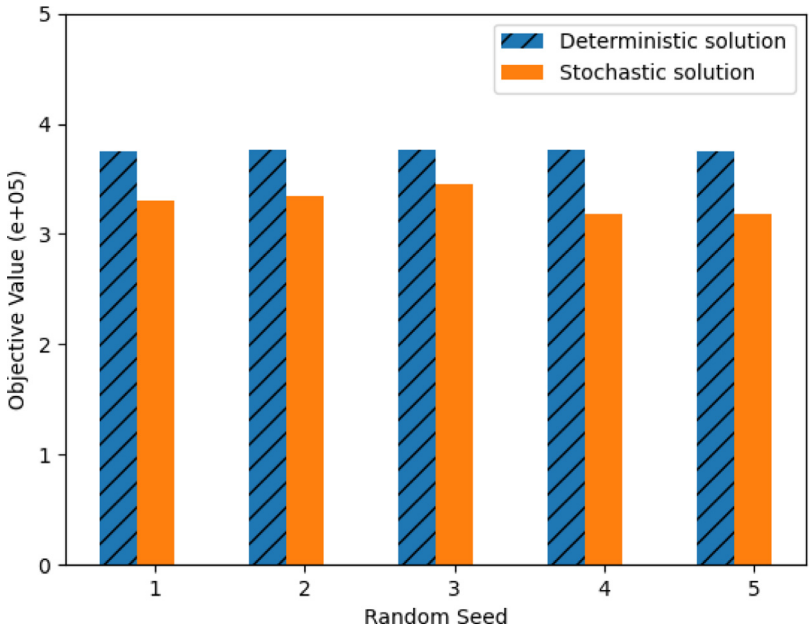

Fig. 7. Objective values of deterministic solution and stochastic solution.

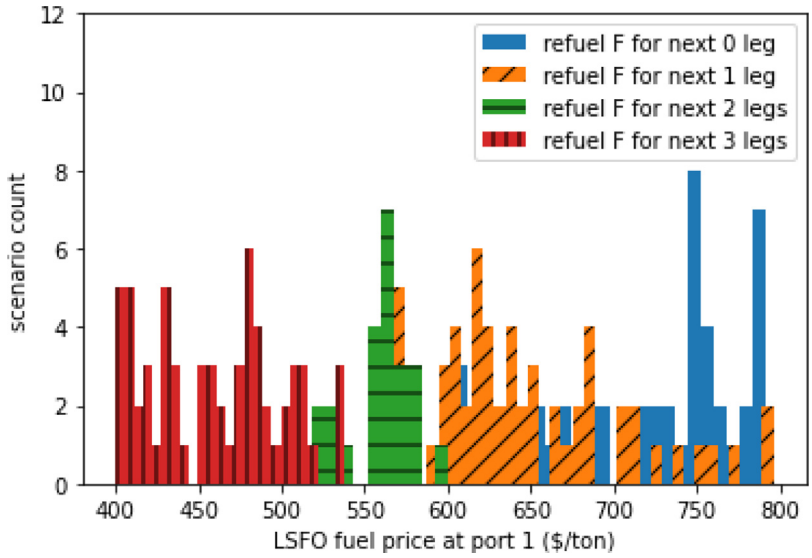

Fig. 8. Observed LSFO fuel price at port 1 for different decisions.

intuition we get from the histogram. For convenience, the decision "refuel LSFO for the following i legs at port 1" is denoted as decision i.

We apply multinomial logistic regression to obtain soft boundaries of LSFO fuel price for different refueling decisions. The soft decision boundary term is defined using a polynomial logistic regression model. Polynomial logistic regression is a statistical method used to model the relationship between a dependent variable and one or more independent variables when the dependent variable has three or more possible outcomes. In this case, a soft decision boundary refers to the model's representation of the tendency to choose a specific fuel type under different fuel prices through computed probabilities, rather than being based on a fixed decision rule. Specifically, the authors employ polynomial logistic regression to analyze the decision-making process for the LSFO refueling. This is a classification problem where the categories are refueling LSFO for the next 0, 1, 2, or 3 segments. The regression model includes the prices of LSFO and LNG as explanatory variables to predict the decision to refuel LSFO at the first port. The model's output consists of probabilities for each category of the refueling decision, and these probability boundaries are referred to as soft decision boundaries. Unlike the hard decision boundary that abruptly change the decision at a specific point or threshold, the soft

Table 3
p-values of Welch's t-test for LSFO fuel price means under different decisions.

Welch's t-test	p-value
0&1	1.586 e-6
1&2	6.104 e-15
2&3	<2.2 e-16

Table 4
AIC of the regression model under different aggregation choice.

Aggregation choice	(0)	(0,1)	(0,1,2)
(3)	224.56	88.09	26.98
(2,3)	198.95	62.20	
(1,2,3)	145.23		

decision boundary allows for a smooth transition of decisions near the boundary, reflecting the continuity and uncertainty of the decision as fuel prices fluctuate. The fuel prices of LSFO and LNG at port 1 are included in the regression model as two explanatory variables, since they are the only two factors that directly influence the refueling decision at port 1.

Aggregation of some refueling decisions is motivated by the significant overlaps that can be identified from the histogram. The resulting Akaike Information Criterion (AIC) of the logistic regression model under different aggregation combinations is shown in Table 4, where combinations from two directions are considered. To be specific, the formula for calculating AIC is $\mathrm{AIC} = 2k - 2\ln(L)$, where k represents the number of parameters in the model, and L represents the maximum likelihood value of the model. When comparing multiple models, AIC values are used to assess which model provides the best explanation while penalizing for model complexity to avoid overfitting. The authors employ AIC values to select the most suitable model (i.e., the way decisions are merged).

Technically, we prefer the model with the lowest AIC, which indicates that the model best fits the given data without overfitting. However, in practice, we also need to consider whether the model we select makes sense in the real world. In this following discussion, we always aggregate decision 0 and 1 unless otherwise noted, since they show the most significant overlapping with each other. In fact, aggregating the two decisions results in the largest AIC reduction. Moreover, logistic regression coefficients estimated in different scenarios can be regarded as different decision strategies, and we are interested in how such strategies respond to the changes of direct and indirect factors.

For convenience, we refer to decision 3 as "radical decision" since it means to purchase all the fuel needed by the ship for the next 3 legs, denote decision 2 as "moderate decision", and denote decision 1 and 0 as "cautious decision" for comparison. In some discussions, we denote decision 2, 1, and 0 as "nonradical decision" as a whole.

The decision boundaries we employed actually represent random decision policies. In Sections 4.3.2 to 4.3.5, this study generates multiple decision boundaries. These boundaries refer to the dividing lines between different decision regions within the decision model. These decision regions typically represent different strategies or action plans, such as in this study, they represent decisions regarding refueling with different types of fuel. The decision boundaries are derived from the results of polynomial logistic regression models and they represent the points at which decisions transition from one type to another when specific prices or other relevant factors change. By analyzing these boundaries, this study investigates how decision-makers' behavior may vary in different scenarios. This approach allows researchers to understand the trends in decision changes when fuel prices fluctuate, environmental policies evolve, or other external factors shift. This is valuable for predicting future decision patterns, assessing the impact of policy changes, or optimizing supply chain decisions, among other applications.

4.3.2. Sensitivity analysis on fuel price

Based on the previous settings, we explore how the mean and variance of LSFO and LNG fuel prices can affect the soft decision boundaries (obtained by multinomial logistic regression).

Firstly, the boundary between radical decision and cautious decision becomes higher as the mean LSFO fuel price increases. In this case, decision 0, 1, and 2 are combined together to present our main conclusion and referred to as cautious decision as a whole. The results are shown in Fig. 9, where the green region represents the radical decision, and the orange region represents cautious or moderate decision. The mechanism behind this phenomenon is simple. Basically, decisions are made by comparing the current price with historical data in the environment, and when it seems relatively favorable, radical decisions are likely to be made. Then naturally, the decision boundary between radical and cautious decisions will adapt to the mean LSFO fuel price.

Besides, it is noteworthy that as mean LSFO fuel price grows larger than \$700/ton, the increasing trend of the boundary slows down. This is because the alternative fuel LNG, with mean \$800/ton and standard variance 100 \$/ton, appears to be more and more appealing as the price of LSFO climbs, thus undermining the attractiveness of a radical LSFO refueling to the decision maker (i.e. the stochastic programming model). The influence of alternative fuel prices will be discussed in a more detailed way later in the same section.

Secondly, variance, i.e. future uncertainty and risk, also has a great impact on the decision-making, as shown in the Fig. 10, with three regions representing radical decision (the region below the solid curve), moderate decision (the region between the solid

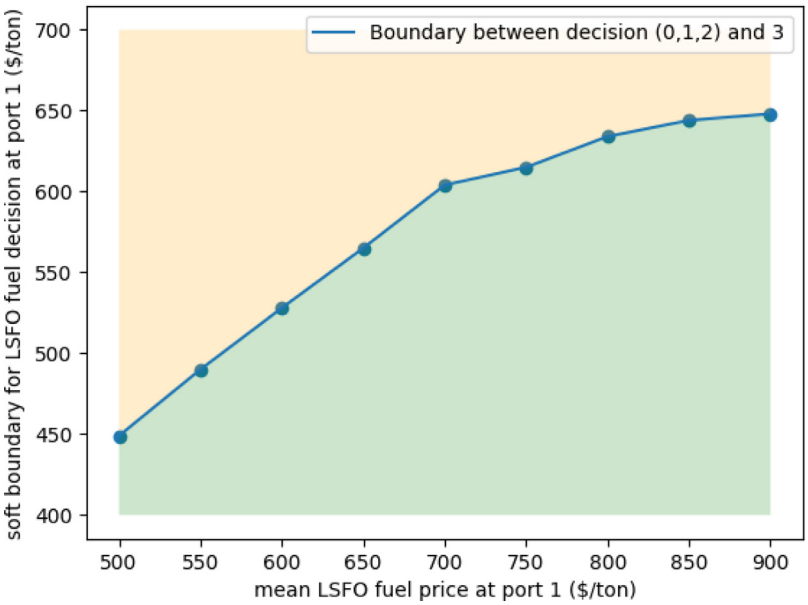

Fig. 9. Decision boundaries against mean LSFO fuel price (at port 1).

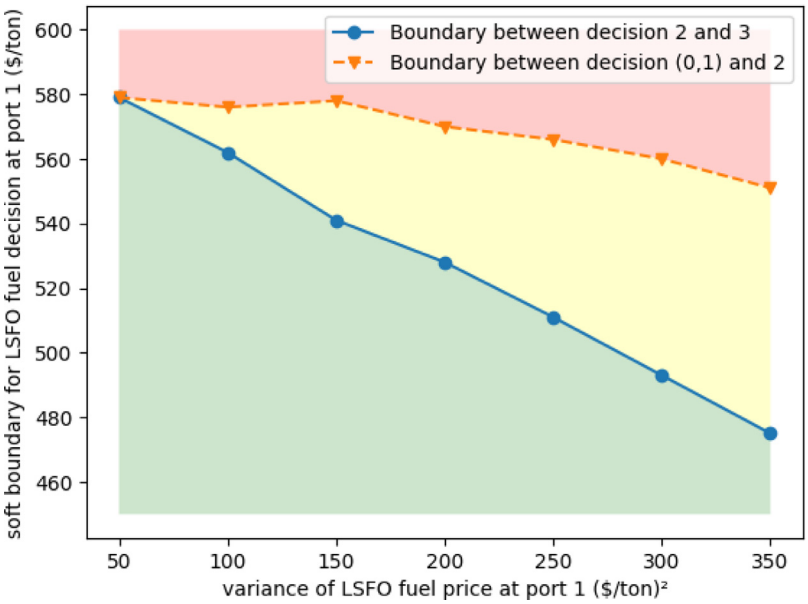

Fig. 10. Decision boundaries against variance of LSFO fuel price (at port 1).

curve and the dashed curve), and cautious decision (the region below the dashed curve). The insight is that the more uncertain the environment is, the shorter the decision period should be. Specifically speaking, as the uncertainty of LSFO fuel price increases, although the mean value of LSFO fuel price remains unchanged, decision makers still prefer to behave conservatively (refuse radical decisions) when the realized LSFO fuel price is not appealing enough, in order to avoid possible risks. In contrast, the moderate decision, which features a relatively short-term refueling plan, becomes popular as uncertainty grows.

Thirdly, we can get an interesting insight into the relationship between decision-making and the mean alternative LNG fuel price from Fig. 11. As the mean LNG fuel price decreases, we are more and more likely to adopt the cautious LSFO refueling decision, even under the LSFO fuel price remains unchanged.

This can be partially explained by the concept of opportunity cost and anchoring effect. On the one hand, low LNG prices may give decision makers the impression that they could have also saved some money if they chose LNG, which implicitly raises the decision maker's expectation of LSFO fuel price. On the other hand, since the decision maker is not omniscient, they are uncertain of whether

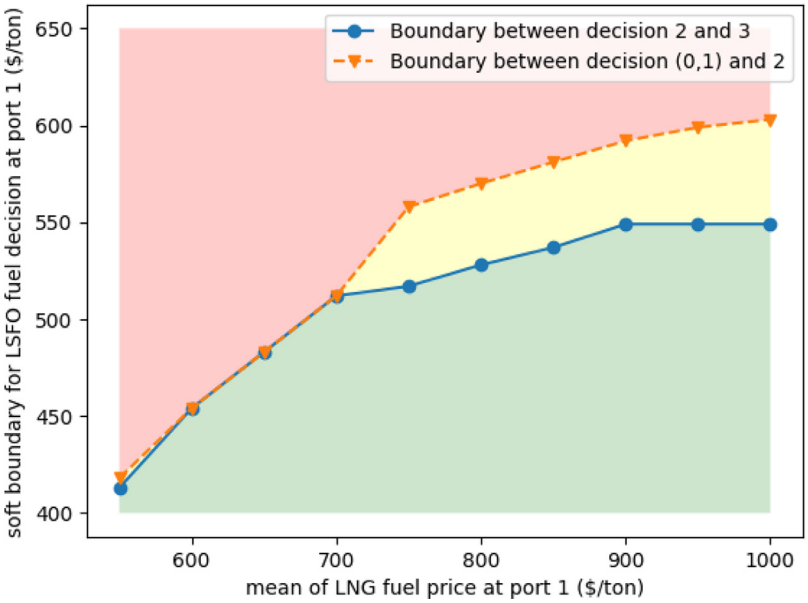

Fig. 11. Decision boundaries against mean LNG fuel price (at port 1).

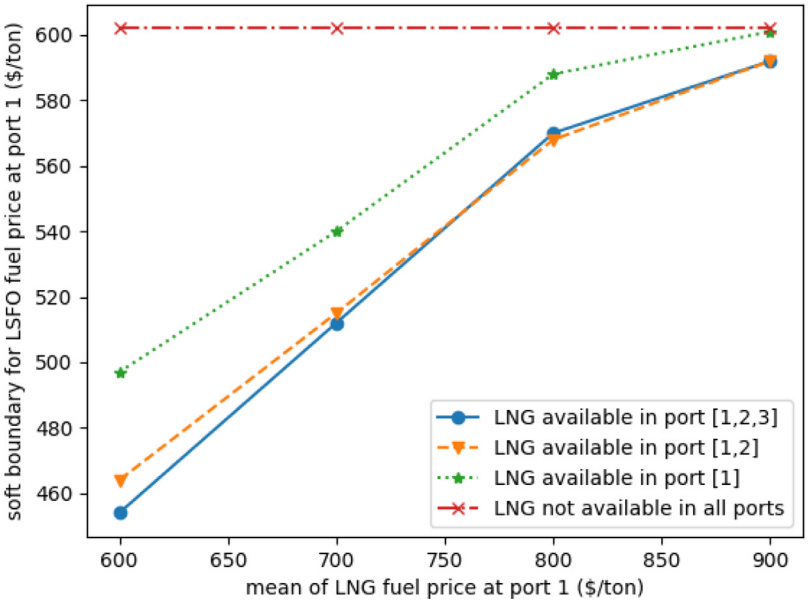

Fig. 12. Decision boundaries against mean LNG fuel price under different LNG availability.

the current LSFO is good enough in the optimal-stopping context. Hence, they may tend to use the observed LNG fuel price as an anchor for convenient comparison. If the LNG fuel price is low, the decision maker will mentally expect the LSFO fuel price to be low as well. We conclude that both effects contribute to the influence of LNG fuel prices on the LSFO refueling decision.

4.3.3. Sensitivity analysis on fuel availability

In the previous discussion, whether LSFO and LNG are available at each port of call is fixed. However, chances are that ports of call in a route may promote the infrastructure construction and make more fuel types available. Hence, sensitivity analysis on fuel availability should be conducted to see how the decision boundaries between radical decisions and nonradical decisions are affected by it. Since in real life, not all ports are equipped with bunkering facilities as mentioned in Section 3.1, the analysis in this section focuses on the LNG availability. Fig. 12 shows how the decision boundary evolves as the LNG availability changes. The dashed and solid lines are close to each other, indicating the decision strategy is insensitive to initial changes of the LNG availability. However, when the opportunity to choose LNG at future ports of call becomes rare (the dotted line), LSFO fuel can be more attractive in

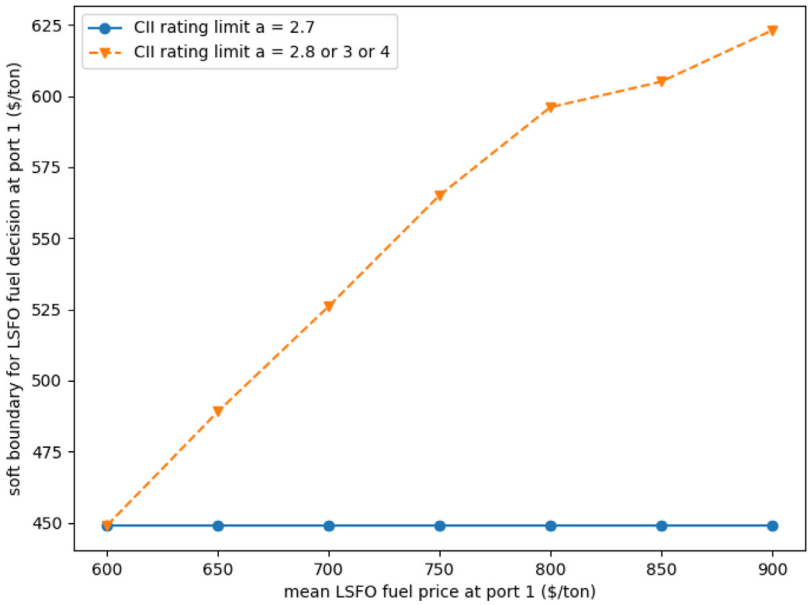

Fig. 13. Decision boundaries against mean LSFO fuel price under different CII rating limits.

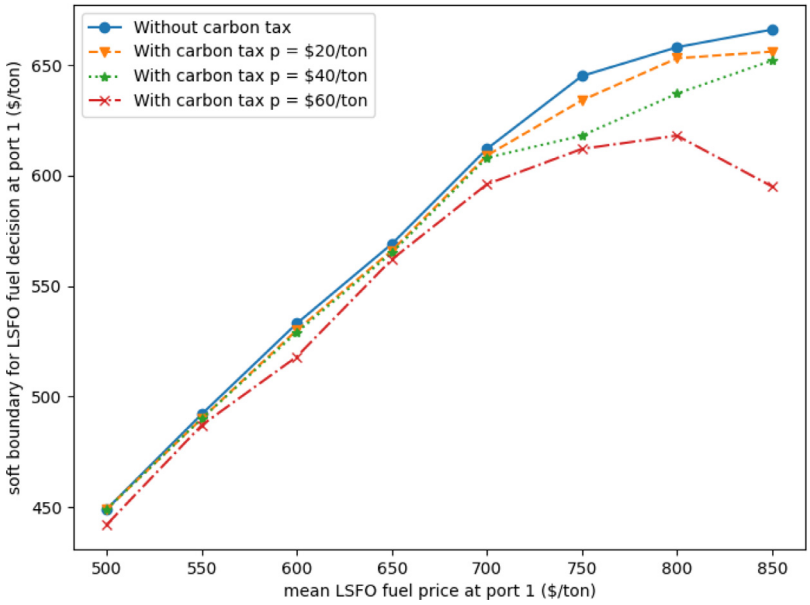

Fig. 14. Decision boundaries against mean LSFO fuel price under different carbon tax.

the decision makers' eyes, increasing the tendency of making radical LSFO refueling decisions. The case where no ports of call can offer LNG fuel (the dashdot line) is a special case, where LSFO refueling decisions are independent of LNG prices. It is not just a coincidence that the dashdot line and other lines meet at the upper right of the figure, because when the LNG fuel price grows larger than $900/ton, it almost loses its competitiveness over LSFO with mean price $600/ton, thus generating decision boundaries as if alternative LNG fuel is not available at all.

4.3.4. Sensitivity analysis on CII rating limit

In this section, we conduct sensitivity analysis on the upper bound of CII rating, with the results shown in Fig. 13. Since the CII rating limit is included in the model through direct constraints (3), CII rating limit becomes a true consideration if and only if constraints (3) become binding constraints, i.e. the constraint is on the verge of being violated. Hence, the decision boundary between radical and nonradical decisions shows a sudden change when CII rating limit a decreases from 2.8 to 2.7 in the 4-port route case. This

indicates that CII rating limit serves as a mandatory requirement instead of a penalty term to the objective function in the refueling decision.

4.3.5. Sensitivity analysis on carbon tax

In this section, the impact of carbon tax on the refueling decisions is explored. We first construct an alternative model without carbon tax based on the model proposed in Section 3.4, and compare the stochastic solutions obtained from the two models under the same scenario. Taking $p = \$40$/ton as an example, the comparison results are demonstrated in Fig. 14, where the solid line represents the soft decision boundaries without carbon tax and the dotted line represents the results with carbon tax $p = \$40$/ton. It is interesting to see that when LSFO fuel price has a low mean value (smaller than \$700/ton), it almost do not make a difference in the refueling decision whether or not we introduce carbon tax, because LSFO fuel is so cheap that the impacts of carbon tax are trivial. However, if LSFO fuel price grows higher than \$700/ton, costs of carbon emission will significantly push decision makers to reconsider the refueling decision and prefer the LNG fuel, which emits less carbon than LSFO on a volume (m^3) basis.

Further, we conduct sensitivity analysis on the carbon tax p to see how decisions can be affected by the strictness of carbon policies, and the results are shown in Fig. 14. In general, our findings suggest that the refueling decision is somewhat insensitive to carbon taxes in this case. We observe that carbon taxes would need to be adjusted to the tens of dollars range to have a significant impact on the refueling decision. When carbon taxes are below \$20/ton, radical LSFO refueling decisions are almost not influenced by the carbon tax. As carbon taxes increase over \$60/ton, carbon tax becomes a true consideration, and a turning point in the boundary of radical LSFO refueling decisions occurs. This indicates that decision makers become unwilling to purchase LSFO fuel with a high price given a strict carbon tax.

5. Conclusion

Due to the growing environmental consciousness and stricter regulations, liner shipping companies are compelled to factor in carbon emissions when selecting refuel types at ports of call. However, fuel type choices are also significantly influenced by fuel prices, which are subject to ongoing fluctuations. Thus, when deciding the refuel type and amount at ports of call, liner shipping companies should consider the trade-off between fuel consumption costs and carbon taxes. To the best of our knowledge, no prior research has studied the coupling of carbon emission considerations and fuel price fluctuations for dual-fuel ships, so this paper proposes a multistage stochastic programming model that tackles the refueling problem for dual-fuel ships to fill this gap.

The contributions of this paper are three-fold. i) This paper proposes a multistage stochastic programming model to tackle the refueling decision problem for dual-fuel ships with CII constraints and fluctuating fuel prices. Various factors, including fuel consumption of main and auxiliary engines, fuel availability, fuel price fluctuations, CII rating limits, and carbon tax costs, are considered in the model. ii) Scenario size selection and moment matching methods are applied to solve the proposed model and a greedy heuristic algorithm is adopted to speed up the process. Numerical results show that the greedy heuristic can greatly reduce the solving time by approximately 80% at the price of only a 5% increase in the achieved objective function value, which implies the potential for applying the proposed model and methods to practical problems, facilitating refueling decisions for practitioners. iii) Several managerial insights are obtained from the sensitivity analyses of crucial model parameters. By applying multinomial logistic regression to the obtained stochastic solutions, soft decision boundaries can be identified between different refueling decisions. We examine how the mean and variance of LSFO prices, the mean of LNG prices, LNG availability at ports of call, CII rating limit, and carbon taxes influence the decision boundary of LSFO in this paper. Our numerical results reveal that (1) The refueling decisions are closely linked to the difference between LSFO and LNG fuel prices, which can be explained by considering the opportunity cost; (2) As the variance of LSFO fuel price increases, radical LSFO refueling decisions are less likely to be made; (3) LSFO becomes more attractive to decision makers when LNG availability decreases; (4) Carbon emission cost becomes a true consideration as carbon taxes increase over \$60/ton. These insights can help practitioners better understand the coupling influence of carbon emissions and fuel price fluctuations in the ship refueling problem.

Future research can focus on three improvement directions of this study. Firstly, more realistic fuel price fluctuations can be considered. Instead of assuming fuel prices follow time-independent normal distributions, time-dependent fuel price time series can be considered, and historical data can be utilized to predict future fuel prices and improve decision-making. Secondly, more factors that affect the fuel consumption rate, such as weather and sea conditions, can be incorporated into the model through forecasting to make the fuel consumption more realistic. Finally, there remains significant scope for future research into the risk and policy implications associated with LNG refueling.

Declaration of competing interest

The authors declare that they have no known competing financial interests or personal relationships that could have appeared to influence the work reported in this paper.

References

ABS (2020) LNG bunkering: technical and operational advisory. (accessed on 15 july 2022) URL https://superlng.adrioninterreg.eu/wp-content/uploads/2020/04/2_FILE.pdf.

Adulyasak, Y., Cordeau, J.F., Jans, R., 2015. Benders decomposition for production routing under demand uncertainty. Oper. Res. 63 (4), 851–867.

Bialystocki, N., Konovessis, D., 2016. On the estimation of ship's fuel consumption and speed curve: a statistical approach. J. Ocean Eng. Sci. 1 (2), 157–166.

Birge, J.R., Louveaux, F., 2011. Introduction to Stochastic Programming. Springer, New York.
Brouer, B.D., Alvarez, J.F., Plum, C.E.M., Pisinger, D., Sigurd, M.M., 2013. A base integer programming model and benchmark suite for liner-shipping network design. Transp. Sci. 48 (2), 281–312.
ClassNK (2021) CII (Carbon Intensity Indicator) (Accessed on 20 January 2023) URL https://www.classnk.or.jp/hp/pdf/activities/statutory/seemp/CII_en.pdf.
Fagerholt, K., Psaraftis, H.N., 2015. On two speed optimization problems for ships that sail in and out of emission control areas. Transp. Res. Part D: Transp. Environ. 39, 56–64.
Feng, Y., Ryan, S.M., 2013. Scenario construction and reduction applied to stochastic power generation expansion planning. Comput. Oper. Res. 40 (1), 9–23.
GEP, 2022. Russia-ukraine war's effects on the oil and gas industry. (Accessed on 01 January 2023) URL https://www.gep.com/blog/mind/russia-ukraine-wars-effects-oil-and-gas-industry.
Ghosh, S., Lee, L.H., Ng, S.H., 2015. Bunkering decisions for a shipping liner in an uncertain environment with service contract. Eur. J. Oper. Res. 244 (3), 792–802.
Heitsch, H., Römisch, W., 2003. Scenario reduction algorithms in stochastic programming. Comput. Optim. Appl. 24 (2-3), 187–206.
Høyland, K., Wallace, S.W., 2001. Generating scenario trees for multistage decision problems. Manag. Sci. 47 (2), 295–307.
Hu, Z., Hu, G., 2018. A multi-stage stochastic programming for lot-sizing and scheduling under demand uncertainty. Comput. Ind. Eng. 119, 157–166.
IMO, 2011. Fourth IMO GHG study 2020-executive summary. (Accessed on 09 January 2023) URL https://www.cdn.imo.org/localresources/en/OurWork/Environment/Documents/Fourth%20IMO%20GHG%20Study%202020%20Executive-Summary.pdf.
IMO, 2018. Initial IMO GHG strategy. (Accessed 20 July 2021) URL https://www.imo.org/en/MediaCentre/HotTopics/Pages/Reducing-greenhouse-gas-emissions-from-ships.aspx.
IMO, 2022. Rules on ship carbon intensity and rating system enter into force. (Accessed on 03 January 2023). URL https://www.imo.org/en/MediaCentre/PressBriefings/pages/CII-and-EEXI-entry-into-force.aspx.
Jin, M., Granda-Marulanda, N.A., Down, I., 2014. The impact of carbon policies on supply chain design and logistics of a major retailer. J. Clean. Prod. 85, 453–461.
Kleywegt, A.J., Shapiro, A., Homem-De-Mello, T., 2001. The sample average approximation method for stochastic discrete optimization. SIAM J. Optim. 12 (2), 479–502.
Kontovas, C.A., Psaraftis, H.N., 2011. Reduction of emissions along the maritime intermodal container chain: operational models and policies. Maritime Policy Manag. 38, 451–469.
Kosmas, O.T., Vlachos, D.S., 2008. Simulated annealing for optimal ship routing. Comput. Oper. Res. 39 (3), 576–581.
Lashgari, M., Akbari, A.A., Nasersarraf, S., 2021. A new model for simultaneously optimizing ship route, sailing speed, and fuel consumption in a shipping problem under different price scenarios. Appl. Ocean Res. 113, 102725.
Lin, Y.H., Fang, M., Yeung, R.W., 2013. The optimization of ship weather-routing algorithm based on the composite influence of multi-dynamic elements. Appl. Ocean Res. 43, 184–194.
Meng, Q., Du, Y., Wang, Y., 2016. Shipping log data based container ship fuel efficiency modeling. Transp. Res. Part B: Methodol. 83, 207–229.
Meng, Q., Wang, S., Andersson, H., Thun, K., 2014. Containership routing and scheduling in liner shipping: overview and future research directions. Transp. Sci. 48 (2), 265–280.
Notteboom, T.E., Cariou, P., 2009. Fuel surcharge practices of container shipping lines: is it about cost recovery or revenue-making? The 2009 International Association of Maritime Economists (IAME) Conference. Copenhagen, Denmark.
Pekic, S., 2022. Hyundai samho picks GTT tank design for four LNG-fueled containerships. (Accessed on 15 July 2022). URL https://www.offshore-energy.biz/hyundai-samho-picks-gtt-tank-design-for-four-lng-fuelled-containerships/.
Ronen, D., 1982. The effect of oil price on the optimal speed of ships. J. Oper. Res. Soc. 33 (11), 1035–1040.
Ronen, D., 2011. The effect of oil price on containership speed and fleet size. J. Oper. Res. Soc. 62 (1), 211–216.
Sha, Y., Zhang, J., Cao, H., 2021. Multistage stochastic programming approach for joint optimization of job scheduling and material ordering under endogenous uncertainties. Eur. J. Oper. Res. 290 (3), 886–900.
Sheng, X., Chew, E., Lee, L., 2015. (s, s) image policy model for liner shipping refueling and sailing speed optimization problem. Transp. Res. Part E: Logistic. Transp. Rev. 76, 76–92.
Ship and Bunker, 2024. (S&B). Global 20 ports average. (Accessed on 13 January 2024) https://shipandbunker.com/prices/av/global/av-g20-global-20-ports-average.
Ship and Bunker 2023. (S&B). World bunker prices. (Accessed on 19 January 2022) https://shipandbunker.com/prices/av/global/av-g20-global-20-ports-average. IFO380,
Wang, C., Xu, C., 2015. Sailing speed optimization in voyage chartering ship considering different carbon emissions taxation. Comput. Ind. Eng. 89, 108–115.
Wang, S., Meng, Q., 2012. Sailing speed optimization for container ships in a liner shipping network. Transp. Res. Part E: Logistic. Transp. Rev. 48 (3), 701–714.
Wang, S., Meng, Q., Liu, Z., 2013. Bunker consumption optimization methods in shipping: a critical review and extensions. Transp. Res. Part E: Logistic. Transp. Rev. 53 (1), 49–62.
Wang, S., Qi, J., Laporte, G., 2022. Governmental subsidy plan modeling and optimization for liquefied natural gas as fuel for maritime transportation. Transp. Res. Part B: Methodol. 155, 304–321.
Wu, Y., Huang, Y., Wang, H., Zhen, L., 2022. Joint planning of fleet deployment, ship refueling, and speed optimization for dual-fuel ships considering methane slip. J. Mar. Sci. Eng. 10 (11), 1690.
Wu, Y., Huang, Y., Wang, H., Zhen, L., 2023. Nonlinear programming for fleet deployment, voyage planning and speed optimization in sustainable liner shipping. Electron. Res. Archive 31 (1), 147–168.
Ytreberg, E., Åström, S., Fridell, E., 2021. Valuating environmental impacts from ship emissions-the marine perspective. J. Environ. Manag. 282, 111958.
Zhen, L., Wang, S., Zhuge, D., 2017. Dynamic programming for optimal ship refueling decision. Transp. Res. Part E: Logistic. Transp. Rev. 100, 63–74.
Zhen, L., Wu, Y., Wang, S., Laporte, G., 2020. Green technology adoption for fleet deployment in a shipping network. Transp. Res. Part B: Methodol. 139, 388–410.
Zincir, B., Deniz, C., 2018. Maritime industry developments related to alternative fuels. In: In Proceedings of INT-NAM, 3rd International Symposium on Naval Architecture and Maritime, pp. 24–25. Istanbul, Turkey